Journal of the European Ceramic Society **18** (1998) 521–526

PII: S0955-2219(97)00163-5
0955-2219/98/$19.00 + 0.00

High Temperature Mechanical Behaviour of Liquid Phase Sintered Silicon Carbide

M. Keppeler,* H.-G. Reichert, J. M. Broadley, G. Thurn, I. Wiedmann and F. Aldinger

Max-Planck-Institut für Metallforschung, Pulvermetallurgisches Laboratorium, Heisenbergstraße 5, Stuttgart, Germany

(Received 4 March 1997; accepted 11 August 1997)

Abstract

Silicon carbide was liquid phase sintered using Y_2O_3 and AlN as sintering additives. A globular grained microstructure was obtained from α-SiC powder whereas a mixture of β-SiC, with a small amount of α-SiC seeds, revealed platelet shaped grains with an aspect ratio of eight. Beside this difference in grain morphology of the α-SiC grains, the phase content of the grain boundary phase is different. The influence of both aspects onto the mechanical behaviour, i.e. four-point bending strength between room temperature and 1400°C and fracture toughness between room temperature and 1100°C, are investigated.

1 Introduction

Due to the very high temperatures needed for solid state sintering of silicon carbide, there is a risk of abnormal grain growth which makes it difficult to control the microstructure and the related mechanical properties of technical materials. In order to reduce sintering temperature, and also to improve the mechanical properties liquid phase sintering similar to that of silicon nitride was applied to silicon carbide.[1–7] Using Al_2O_3–Y_2O_3 which is the most common additive system for Si_3N_4, the weight loss was high due to reactions of silicon carbide with the oxides at sintering temperature (approximately 1900°C). Therefore a powder bed was necessary for densification, which is not practical for industrial use. Using an additive system consisting of Y_2O_3 and AlN, a better sintering behaviour was found.[1,6,7] Due to the high stability of this additive system a powder bed was not needed anymore and the weight loss during sintering was reduced. Other additive systems like Al_2O_3 and Al_4C_3 have been tested by Jou and Virkar.[4]

Of special interest is the similarity to silicon nitride, that the microstructure of liquid phase sintered silicon carbide can be controlled by using the β- to α-phase transformation.[5-7] By varying the α-/β-SiC ratio in the starting powder either globular or platelet shaped microstructures can be produced. During sintering β-SiC dissolves in the liquid phase and reprecipitates at existing α-SiC seeds in the hexagonal crystal structure. Due to the hexagonal structure of α-SiC anisotropic grain growth results in a platelet structure. This sintering of β-SiC powder, containing a defined number of α-SiC seeds, reveals α-SiC platelets embedded in a grain boundary phase providing a substantial reinforcement as compared to the globular type microstructures. The motivation for the present work was to study the high temperature mechanical properties of such materials.

2 Experimental

2.1 Sample fabrication

Green bodies were produced from high purity powders of α-SiC (Lonza), β-SiC (H. C. Starck), AlN (H. C. Starck) and Y_2O_3 (H. C. Starck) using a conventional powder technology process. The amount of additive phase (10 vol%) as well as its composition with a molar ratio of AlN to Y_2O_3 of 3 : 2, was kept constant. To allow for the development of the platelet reinforced liquid phase sintered silicon carbide, a composition of 1 wt% α-SiC and 99 wt% β-SiC was used as the starting material. Very fine grained equiaxed silicon carbide ceramics were produced, for comparison, by using pure α-SiC starting powder. The powder mixtures were

*To whom correspondence should be addressed.

prepared by attrition milling in isopropanol with Si_3N_4 milling media for 4 h using a polyethylene container and stirrer. The slurry was separated from the milling media via a sieve chain and subsequently dried in a vacuum evaporator. Completely dried mixtures were obtained after 48 h at 65°C in a drying chamber. Finally the processed powder was sieved, to obtain granules with a maximum diameter of 160 μm, and cold isostatically pressed at a pressure of 625 MPa into samples with the dimensions $70\times20\times10\,mm^3$. Sintering was performed in a gas-pressure furnace (KCE Kessel GmbH, Rödental) with a graphite heating element in a nitrogen atmosphere. Ceramics comprising of pure α-SiC starting powder were sintered at 1980°C and 30 min dwell time under slight nitrogen overpressure (0·2 to 0·3 MPa). They achieved full density with a weight loss of about 2%. This weight loss can be correlated to the SiO_2 content in the silicon carbide starting powder. Ceramics comprising of a mixture of α/β-SiC starting powder were densified at 1990°C and 30 min dwell time at atmospheric pressure, followed by a pressure sintering cycle of 30 min at the same temperature under 10 MPa N_2 to achieve complete densification. After this treatment the pressure and the temperature were lowered and held at 0·5 MPa and 1970°C, respectively, for 6 h to allow for the complete $\beta\rightarrow\alpha$-SiC phase transformation. With these treatments the ceramics achieved also full density with a weight loss of about 4·5%. The globular and platelet shaped microstructures of both as sintered materials are shown by representative SEM micrographs in Figs 1 and 2. Grain size characteristics of both materials were examined by evaluation of 1000 grains in SEM micrographs of each material with an image processing software (ImageC, Imtronic) and are summarised in Table 1.

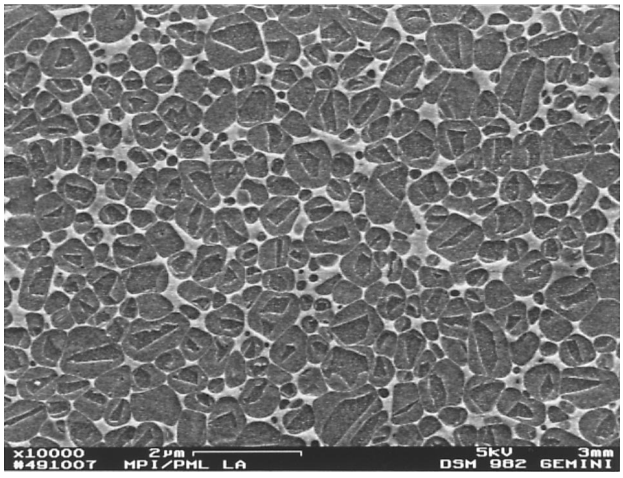

Fig. 1. Typical microstructure of a ceramic sintered from pure α-SiC starting powder. The core/rim structure due to solution/reprecipitation can be seen clearly.

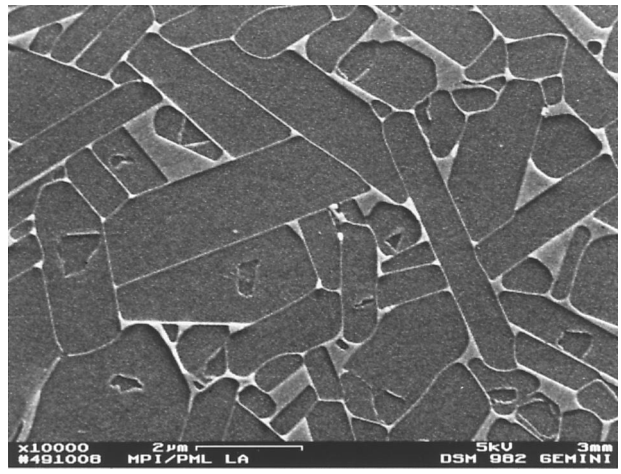

Fig. 2. Typical microstructure of a ceramic sintered with a ratio of 1 wt% α-SiC and 99 wt% β-SiC starting powder.

Stereological examination of the platelet shaped α-SiC (1000 grains evaluated with the software Stereology, Fa. Imtronic) revealed an aspect ratio of 8. Figures 3 and 4 represent typical X-ray diffraction patterns (Siemens D5000, Cu K_α radiation) of the two materials investigated. The phase content of both materials are given in Table 2. Beside a difference in the silicon carbide polytypes the grain boundary phases are different due to the additional heat treatment after sintering. For the strength measurements bar-shaped samples were ground to a size of $3\times4\times25\,mm^3$. The tensile surface of the bars was polished to a 3 μm diamond finish and the tensile edges beleved to avoid stress concentrations and large edge flaws caused by sectioning. For the investigations of the fracture mechanics, cylinders of 15, 12 and 10 mm diameter were prepared from the sintered bodies using diamond core drills. The cylinders were cut into discs which were ground to a thickness of 300 μm and polished to a 3 μm diamond finish. A 3 mm long radial oriented notch was cut with a 100 μm diamond saw blade into each disc-shaped specimen.

2.2 Bending strength measurements

Four-point bending strength measurements were performed at temperatures between room temperature and 1400°C in air. At each temperature at least six specimens were tested. The tests were performed heating up the specimens by avoiding thermal shock and a dwelltime of 10 min to ensure

Table 1. Morphology of α-SiC grains in globular and platelet-containing silicon carbide

Material	*Median grain-size*	*Range of grain-size*	*Aspect ratio*
Globular SiC	1 μm	0·5–1·4 μm	1
Platelet SiC	6 μm	1·4–8 μm	8

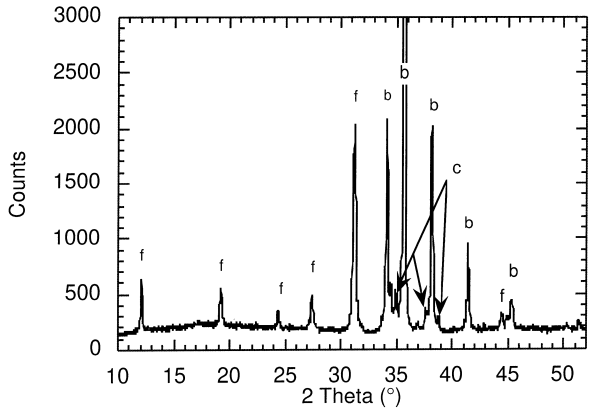

Fig. 3. Diffractograph of a sintered pure α-SiC powder derived material.

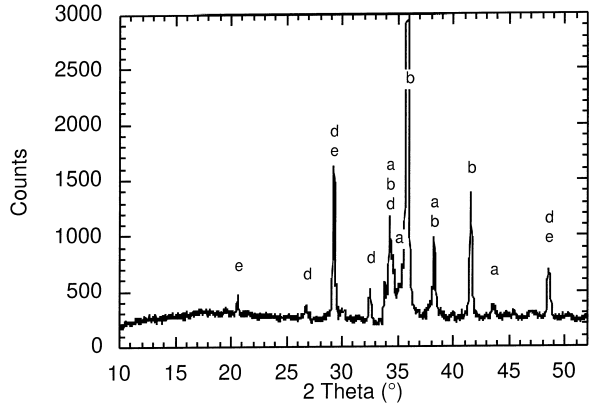

Fig. 4. Diffractograph of a sintered and annealed α-/β-SiC powder mixture derived material.

a homogeneous temperature when tested. The samples were loaded with a constant cross head displacement rate of 0·1 mm min^{-1}.

2.3 High-temperature fracture toughness measurements

A thermal shock testing method developed by Schneider and Petzow[8] was used to study the crack propagation of SiC in the temperature range between 400 and 1100°C. The disc-shaped samples were heated by means of heat radiation from a tungsten lamp or a 100 W Nd–YAG laser. While the tungsten lamp was used for measurements up to 900°C, the laser was used for tests in the temperature range between 900 and 1100°C. The radiation was focused onto the middle of the discs, resulting in a time-dependant axial symmetric temperature field which was measured with an IR pyrometer. As the thermal radiation was continuously increased during the tests, controlled

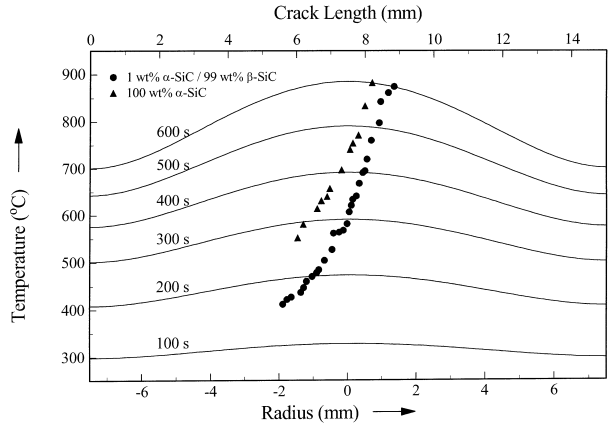

Fig. 5. Temperature profiles for different heating times and crack tip temperatures for different crack lengths.

heating ramps were performed. Figure 5 shows the temperature profiles for different heating times. Crack propagation starts from the notch during heating when the fracture toughness of the materials is exceeded. After short unstable crack initiation, stable crack propagation occurs and can be observed in situ with a microscope. The stress intensity factor K_I of the radially oriented edge cracks was calculated using the weight function method[8,9] and is shown in Fig. 6. K_I is dependant on Young's modulus and the thermal expansion coefficient. Young's Modulus was measured at room temperature with the pulse echo method. It was approximated to be temperature independant up to 900°C. A differential dilatometer was used to determine the thermal expansion coefficient in a temperature range of 400 to 1200°C. It was found that Young's modulus of 390 GPa and thermal expansion coefficient of $5{\cdot}4\times10^{-6}$ K^{-1} were the same for both materials. In addition to stable crack propagation subcritical crack growth was investigated at 1100°C by holding this temperature for 60 min.

3 Results

Figure 7 shows the results of the bending strength measurements between RT and 1400°C. The material with the globular microstructure showed a constant strength of 564 ± 15 MPa from room temperature up to 1000°C. At 1200°C the bending strength increases to 725 ± 68 MPa followed by a sharp decrease to 324 ± 56 MPa at a temperature of 1400°C.

Table 2. Phase content of the sintered α-SiC and α-/β-SiC materials detected by X-ray investigations

Material	*SiC(4H) (a)*	*SiC (6H) (b)*	*SiC (15R) (c)*	*Y_2SiO_5 (d)*	*Y_2O_3 (e)*	*$Y_{10}Al_2Si\cdot O_{18}N_4$ (f)*
Globular SiC		x	x			x
Platelet SiC	x	x		x	x	

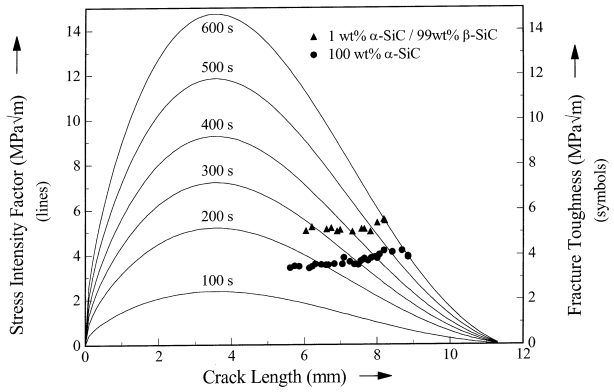

Fig. 6. Stress intensity factors and fracture toughness for different crack lengths.

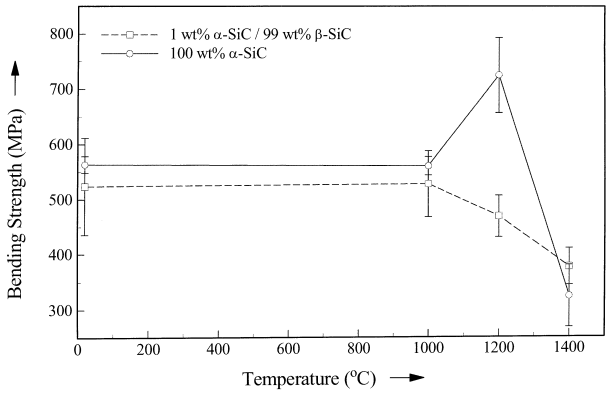

Fig. 7. Bending strength versus temperature for globular and platelet reinforced SiC.

The bending strength of the material with platelet-shaped microstructure was also found to be constant between room temperature and 1000°C with a value of 524 ± 88 MPa and therefore in the same range as the globular material. However in contrast to the pure α-SiC material, above 1000°C the strength continuously decreased down to 377 ± 33 MPa at 1400°C.

The fracture toughness of the globular material in the temperature range between 400 and 900°C was measured to be between 3·4 and 4·1 MPa$\sqrt{\text{m}}$ whereas that of the platelet material was found to be between 5·0 and 5·5 MPa$\sqrt{\text{m}}$ (Fig. 6).

4 Discussion

The increase of the bending strength of the α-SiC-material in the temperature range between 1000 and 1200°C, is comparable to the behaviour of silicon nitride measured by Noakes[10] with an increase of 50 MPa. The authors explained this behaviour by a softening and a subsequent stress relief through viscous flow of the grain boundary phase. To investigate subcritical crack propagation in this temperature range, thermal shock tests were performed with the disc-shaped specimen. *In situ* observation of the crack tip at 1100°C with an optical microscope revealed a shortening of the crack during a 60 min test. Figure 8 shows the crack path near the crack tip after subcritical crack growth. On the left hand side and on the right hand side of the micrograph pore shaped remainders of the crack can be seen. In between these holes the crack path is completely filled with a glassy secondary phase. The closing of the crack was observed on a length of 50 μm. The glass formation is due to the oxidation of the crack borders. Energy dispersive X-ray spectroscopy (EDX) revealed that the glassy phase in the crack path consists mainly of SiO_2, which is an oxidation product of SiC, in contrary to the secondary phase in triple grain junctions. The complete results of EDX-measurements are given in Table 3. At a higher magnification beside the glassy phase fine silicon carbide grains (5) can be seen along the filled crack path (Fig. 9). Obviously the viscosity of the glassy phase is reduced locally due to oxidation of the SiC material so that the crack can be completely filled by viscous flow. Therefore we assume that oxidation is the major mechanism which closes flaws and microcracks and blunts crack tips that are exposed to air. This conclusion is in agreement with results of Lanin *et al.*[11] who investigated the temperature-dependence of the bending strength for porous silicon nitride. An increase of the bending strength between 900 and 1200°C was found when the testing was performed in air, while a decrease was identified in nitrogen.

In contrast to the fine grained globular material, the platelet material showed a decrease of the bending strength between 1000 and 1200°C, due to different oxidation behaviour. Figure 10 shows the

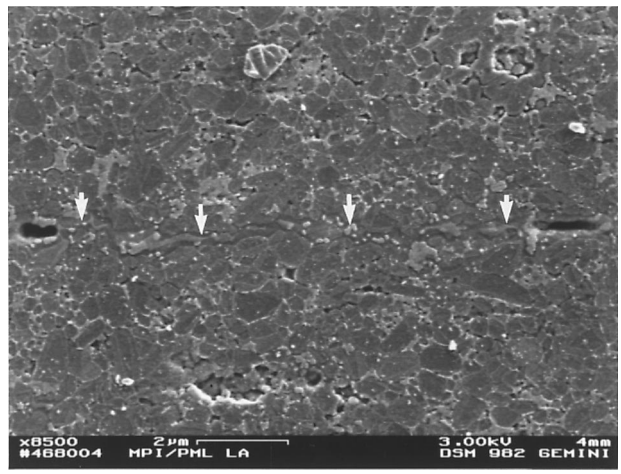

Fig. 8. Crack path near the crack tip in the globular SiC material after 30 min subcritical crack growth at 1100°C. Crack propagation from left to right. Surface prepared by polishing and plasma etching. Light grey particles are remainders of the surface oxidation layer not remove during polishing.

Table 3. EDX-analysis of the secondary phase in the crack path formed after 60 min subcritical crack growth at 1100°C and in the triple grain junctions

Element	*Crack path 1. measurement atomic %*	*Crack path 2. measurement atomic %*	*Triple grain junction atomic %*
O	66	60	40
Al	1	1	2
Si	31	38	50
Y	2	1	8
Total	100	100	100

crack path near the crack tip after 60 min subcritical crack growth at 1100°C in the thermal shock test. The crack is not filled with glassy phase. At a higher magnification an oxidation layer formed on the surface of the SiC grains can be seen (Fig. 11). The oxidation rate is not high enough to heal the crack during the testing time. Therefore in four-point bending tests curing of flaws by oxidation is impossible due to the short time the specimens are exposed to the high temperatures. Thus the softening of the grain boundary phase in this temperature range decreases the bending strength. Figure 11 reveals the ductile fracture of the secondary phase.

Although the additive system was identical for both materials, the phase composition after sintering is different (Table 2). While in the globular material crystalline $Y_{10}Al_2Si_3O_{18}N_4$[12] could be detected by X-ray diffraction, samples of the platelet-material revealed Y_2O_3 and Y_2SiO_5. Grain boundaries of the crystalline secondary phase can be seen in Fig. 11 marked by arrows. Due to the different grain boundary phase contents the oxidation behaviour in the temperature range between 1000 and 1400°C is different. The oxidation rate is lower in the platelet material and therefore cracks can not be healed as observed with the globular

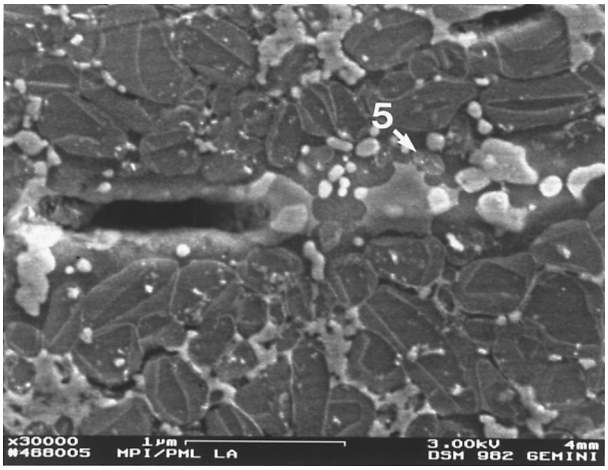

Fig. 9. Detail of the crack path in the globular SiC material filled with secondary phase after 60 min subcritical crack growth at 1100°C.

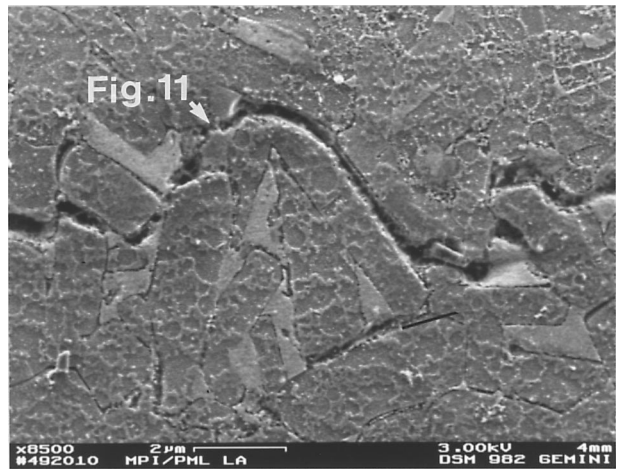

Fig. 10. Crack path in the platelet SiC material after 60 min subcritical crack growth at 1100°C. Crack propagation from right to left. Surface prepared by polishing and plasma etching.

material. However further investigation is necessary to understand this behaviour. Currently TEM investigations are in progress and will be published elsewhere. The increase of the fracture toughness of the platelet-containing material, as compared to the globular material, is obvious from the crack path.[5–7] Figure 12 shows a room temperature crack path in the platelet material. Crack bridging (1) crack deflection (2) and mechanical interlocking (3) were observed as major toughening mechanisms. Platelets with an orientation normal to the crack were broken without any debonding (4), indicating that pull-out of platelets is not a toughening mechanism. The crack path of the globular material is mainly straight (Fig. 13). Only crack bridging was observed. Due to the different grain size and aspect ratio of the grains the toughening effect of these crack bridges is much smaller than in the α-/β-SiC material.

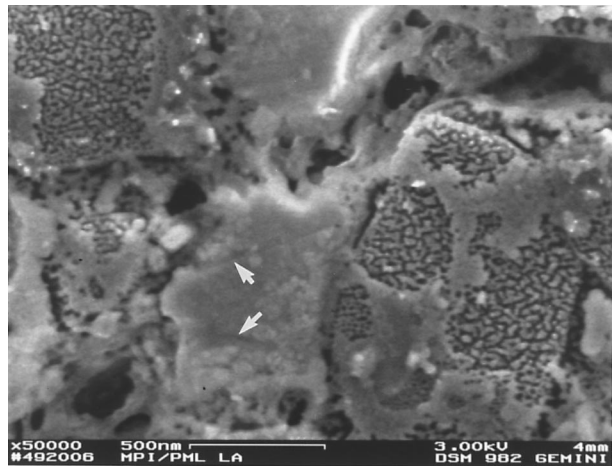

Fig. 11. Detail of the crack path in the platelet SiC material showing ductile fracture of the secondary phase after 60 min subcritical crack growth at 1100°C. Arrows indicate grain boundaries of the crystalline secondary phase.

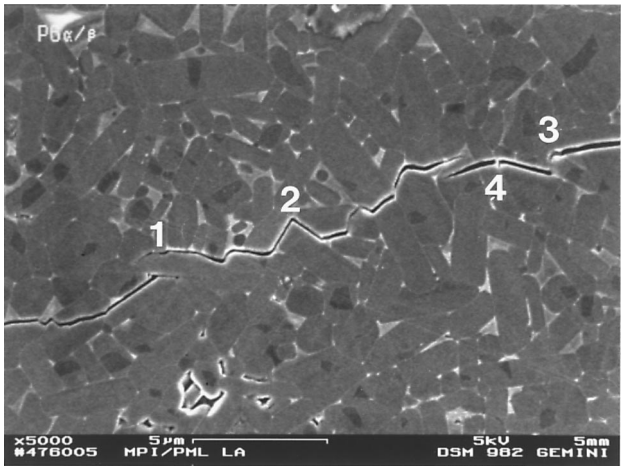

Fig. 12. Room temperature crack path in the *in situ* platelet reinforced SiC material, induced by Vickers indentation. Major toughening mechanisms are crack bridging (1) crack deflection (2) and mechanical interlocking (3) while there is no pull-out of platelets (4).

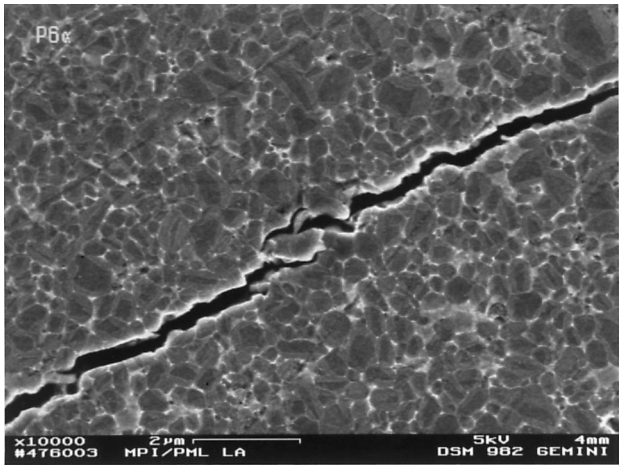

Fig. 13. Room temperature crack path in the globular SiC material, induced by Vickers indentation.

5 Conclusions

Liquid phase sintering offers the possibility to control the microstructure and the properties of silicon carbide ceramics. Globular SiC can be produced by liquid phase sintering from α-SiC powder and in situ platelet reinforced SiC from a mixture of 99% β-SiC and 1% α-SiC. Both materials have similar bending strength between room temperature and 1000°C. The globular material reveals an increase of strength in the temperature range between 1000 and 1200°C due to the healing of flaws and surface cracks with a glassy phase formed by oxidation of SiC. The bending strength of the platelet material decreases above 1000°C due to softening of the grain boundary phase. The fracture toughness of the in situ platelet reinforced material is higher due to crack bridging, crack deflection and mechanical interlocking.

References

1. Chia, K. Y., Lewiston, N. Y. and Boecker, W. D. G., Silicon carbide bodies having high toughness and fracture resistance and method of making same. United States Patent No. 5,298,470.
2. Suzuki, K., Pressureless-sintered silicon carbide with addition of aluminum oxide. In *Silicon Carbide Ceramics–2*, ed. S. Somiya and Y. Inomata. Elsevier Applied Science, London, 1991, pp. 163–182.
3. Mulla, M. A. and Krstic, D., Low-temperature pressureless sintering of β-silicon carbide with aluminum oxide and yttrium oxide additions. *Ceram. Bull.*, 1991, **70**(3), 439–443.
4. Jou, Z. C., Virkar, A. V. and Cutler, R. A., High temperature creep of SiC densified using transient liquid phase. *J. Mater. Res.*, 1991, **6**(9), 1945–1949.
5. Padture, N. P., In situ-toughened silicon carbide. *J. Am. Ceram. Soc.*, 1994, **77**(2), 519–523.
6. Nader, M., Examination on graingrowth phenomena in liquid phase sintered SiC-ceramics and possibilities of variation of the morphology. Ph.D. thesis, University of Stuttgart, Germany, 1995.
7. Wiedmann, I., Nader, M., Hoffmann, M. J. and Aldinger, F., Liquid phase sintering of silicon carbide. Proceedings of Werkstoffwoche '96, Symposium 7, eds. F. Aldinger, and H. Mughrabi, DGM Informationsgesellschaft, Frankfurt, Germany, 1996, pp. 512–520.
8. Schneider, G. A. and Petzow, G., Thermal shock testing of ceramics—a new testing method. *J. Am. Ceram. Soc.*, 1991, **74**(1), 98–102.
9. Schneider, G. A., Magerl, F., Hahn, I. and Petzow, G., In situ observations of unstable and stable crack propagation and R-curve behaviour in thermally loaded disks. In *Thermal Shock and Thermal Fatigue Behavior of Advanced Ceramics*, ed. G. A. Schneider and G. Petzow. Kluwer Academic, The Netherlands, 1993, pp. 229–244.
10. Noakes, P. B. and Pratt, P. L., High-temperature mechanical properties of reaction-sintered silicon nitride. In *Special Ceramics 5*, ed. P. Popper. British Ceramic Research Association, Stoke-on-Trent, 1972, pp. 299–310.
11. Lanin, A. G., Antsiferov, V. N. and Gilyov, V. G., Manufacturing features, structure and properties of high-porous Si_3N_4-ceramics and SiAlONs.. *Proceedings of the International Conference on Silicon Nitride-Based Ceramics, Key Engineering Materials*, 1994, **89–91**, 653–657.
12. Wills, R. R., Reaction of Si_3N_4 with Al_2O_3 and Y_2O_3. *J. Am. Ceram. Soc.*, 1975, **58**, 335.